ELSEVIER

Journal of Hazardous Materials 40 (1995) 85–108

JOURNAL OF HAZARDOUS MATERIALS

# Further development of a model for dense gas dispersion over real terrain

R.P. Cleaver*, M.G. Cooper, A.R. Halford

*British Gas plc, Research and Technology, Gas Research Centre, Ashby Road, Loughborough, Leicestershire, LE11 3QU, UK*

Received 5 November 1993; accepted in revised form 8 July 1994

**Abstract**

This paper addresses the development of a computer-based mathematical model for the prediction of the dispersion of dense gas. The basic model for dispersion over flat terrain is outlined and its performance is illustrated by comparison with a range of field trial information. It is then shown how a number of separate algorithms for the effects of obstacles on dispersion can be combined into a single algorithm that can be applied to enable predictions to be made for dispersion over a typical industrial site. The complete model is then compared with results from a more limited range of field trial and wind tunnel experiments. The paper ends with a discussion on both the usefulness and also the limitations of this approach.

## 1. Introduction

Over the past twenty years, much effort has been devoted towards improving the capability to predict how a denser-than-air gas cloud disperses in the atmosphere. Mathematical modelling, field trials and idealised laboratory or wind tunnel studies have all been undertaken. This has led to the development of a number of computer-based models of the integral type that may be used for routine hazard analysis purposes. The level of agreement of these models with experimental data for dispersion over flat, uninterrupted terrain has been demonstrated, for example, by Hanna et al. [1]. Whilst opinions may differ as to the precise interpretation of comparison exercises such as these, they do establish an independent methodology that anyone can apply and against which alternative model developments can be tested. They also indicate to a wider audience some form of standardised attainment targets for agreement between theory and experiment that may be achieved by the best of the models.

* Corresponding author.

*SSDI* 0304-3894(94)00081-6

More recently, there has been a growing trend towards developing models that take account of variations of the underlying terrain and the presence of obstacles. This is demonstrated by the recent CEC-sponsored field-scale work of Nielsen [2], the wind tunnel work from the Warren Spring Laboratory [3] and the University of Hamburg [4], and algorithm developments such as those proposed, for example, by Britter et al. [5] or Webber and Jones [6].

In the context of the dispersion of flammable gases, the reasons for this interest follow from a desire to make a full assessment of the potential hazards posed by these clouds. To estimate the overpressures that are likely to be generated in the event of their ignition requires not only a better knowledge of the dispersion or flammable 'footprints' of such clouds, but also a knowledge of the inventory within the regions of obstacles or confinement. The studies reported by Harris and Wickens [7], for example, have shown that the presence of repeated obstacles or confinement within flammable clouds has a crucial role to play in the acceleration of the flame front and hence the generation of damaging pressures.

The purpose of this present paper is twofold. Firstly, it is to present information on the performance of an integral type of dense gas dispersion model with basic datasets obtained from flat terrain field-scale experimental programmes. The model itself results from the further development and review of the model proposed by Carpenter et al. [8]. The model equations are presented separately in Appendix A. There is little in this part of the work that is novel or indeed different from the many other similar models that have been reported earlier. However, using measures similar to those proposed by Hanna et al. [1], we are able to present a systematic comparison of the performance of this model in Section 2 and demonstrate its strengths and weaknesses.

The second purpose of the paper is to give further details of a single algorithm that may be used to account for the presence of a variety of obstacles in the flow field. Comparison of the performance of this model with available field-trial data is presented in Section 4. It is shown that by including the submodel for the effects of an obstacle, better agreement with the data is obtained. Hence, a better estimate of the inventory in obstructed regions is provided, although the details of the concentration distribution in the immediate neighbourhood of the obstacles are not predicted. The paper concludes with a brief discussion of the findings of the comparison of the model with data and suggests areas where further work is required.

## 2. Model for dispersion over flat terrain

The equations of the model are given in the Appendix A. The model belongs to the class of similarity or integral type of models. These models aim to use physically based simplifying assumptions in order to reduce the governing set of equations for the dispersion to a series of linked, ordinary, rather than partial, differential equations. This presents a great gain, both in terms of the methods that can be employed and also the time taken to obtain a solution to the equations. This is counterbalanced by a loss of detail in the solution. The model may also be restricted to a limited number of scenarios for which the simplifying assumption is valid.

In line with the more recent, and successful, integral model developments such as those of Puttock [9], Havens [10] or Webber et al. [11], concentration profiles are imposed on the dispersing cloud, thereby avoiding artificial discontinuities in predictions once the passive or atmospheric dispersion-dominated phase is reached. A separate source blanket type of algorithm is included for continuous low momentum sources such as may arise from evaporating or boiling pools of liquefied fuels. The inclusion of a horizontal momentum equation, albeit in a highly simplified and approximate form, means that the model can also use the results from a similar type of integral model for jet dispersion as initial conditions. This enables the model to handle the jet type of releases that can occur from pressurised storage.

As with the models of Puttock [9] and Havens [10], allowance is made for the entrainment due to the convective motions set up by the heat transfer from the underlying surface to the cloud. As suggested by Witlox [12], allowance is made for the breakdown of the organised gravity head at the edges of the cloud, although the terms representing this follow the suggestions of Britter [13].

The procedure followed in calibrating the code was as follows:

(i) Data from the ambient temperature Thorney Island instantaneous field trials were first used to determine the approximate values for the gravity spreading and edge entrainment coefficients.

(ii) Data from the ambient temperature Thorney Island continuous and the Shell Maplin LPG field trials were then used to determine the approximate values for the top entrainment coefficients.

(iii) Data from the Shell Maplin LNG and Burro and Coyote LNG field trials were then used to determine approximate values for the constants appearing in the expressions representing the convection-induced entrainment.

(iv) Finally, the model was compared with all the datasets and similar measures to those employed by Hanna et al. [1] were used to finalise the optimum set of model constants. (The report by Hanna et al. [1] contains references to all the field trials referred to above.)

It should be noted that in each case the original data reports were used as sources of experimental data and for the input conditions to the model. For the instantaneous release experiments, the peak value of the concentration measured at any location was compared with the peak value predicted at ground level. For continuous releases, the effect of the different time averaging periods on the passive dispersion parameters were taken into account, using power-law type of relationships proposed by Wilson [14].

Fig. 1 presents a comparison of the observed concentrations with the predicted concentrations from all the trials listed in Table 1. The solid line at 45° to the axes represents a line of perfect agreement between model and experiment, whereas the dashed lines represent differences of a factor of two between them. As would be expected, given the calibration of the model against this data, the model predictions lie evenly either side of the line of perfect agreement and over 90% of the predictions are within a factor of two of the data. This information is presented in a different form, where the ratio of observed to predicted concentration is plotted against absolute humidity in Fig. 2(a), against windspeed in Fig. 2(b), and against assumed atmospheric

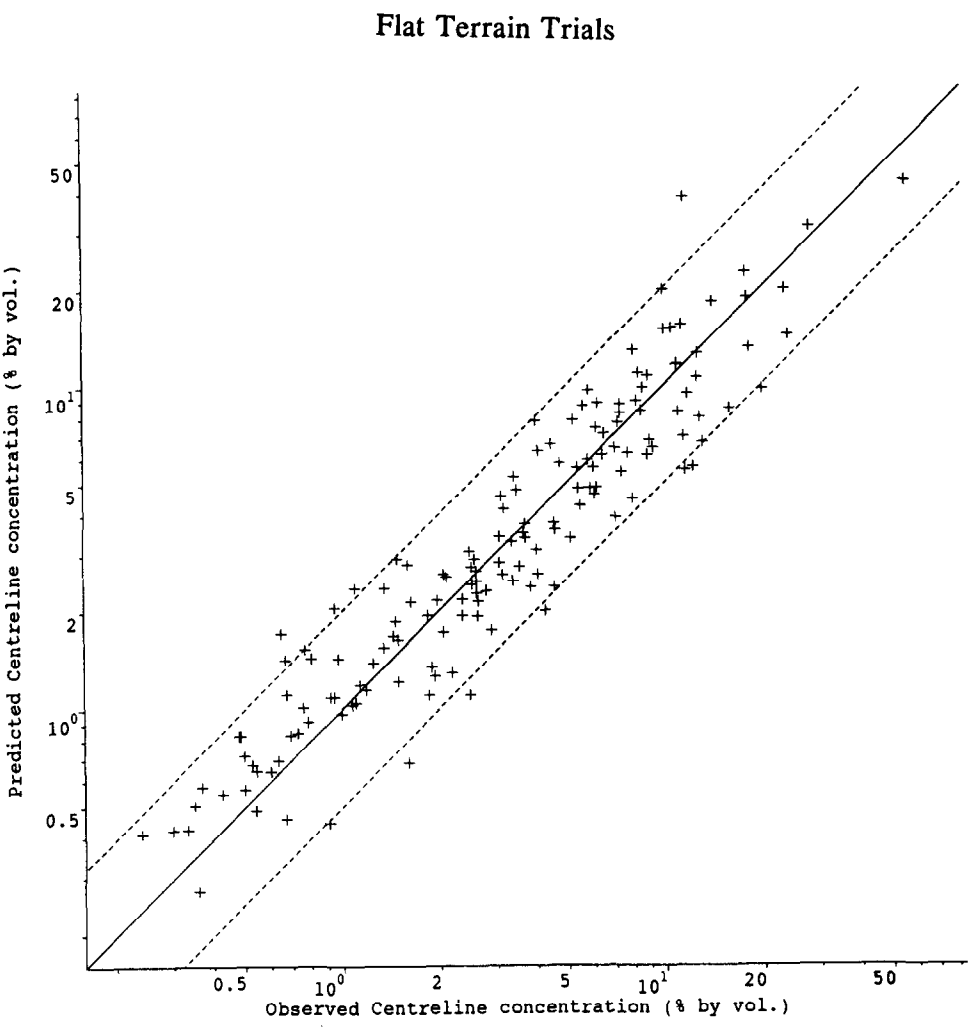


Fig. 1. A plot of the measured against the predicted concentrations for the trials listed in Table 1.

stability category in Fig. 2(c); the sensitivity to the different experimental configurations is shown in Fig. 2(d). There is little evidence for any systematic bias of the predictions of the model in these figures.

More data are available from the Phase 1 Thorney Island trials than from the other test series, and here it is possible to make comparisons with visual observations of the cloud heights and widths. A similar level of agreement was found to that demonstrated by Carpenter et al. [8], with essentially an earlier version of this model. For the other field trials, only cloud widths have been compared and these appear to be satisfactory.

Table 1
Field trials used to calibrate the flat terrain model

| Series and Test No. | | Material | Release type |
|---|---|---|---|
| Maplin Sands | 27 | Methane | Continuous |
| Maplin Sands | 29 | Methane | Continuous |
| Maplin Sands | 34 | Methane | Continuous |
| Maplin Sands | 35 | Methane | Continuous |
| Maplin Sands | 43 | Propane | Continuous |
| Maplin Sands | 46 | Propane | Continuous |
| Maplin Sands | 47 | Propane | Continuous |
| Maplin Sands | 49 | Propane | Continuous |
| Maplin Sands | 50 | Propane | Continuous |
| Maplin Sands | 54 | Propane | Continuous |
| Thorney Island | 6 | Freon/nitrogen | Instantaneous |
| Thorney Island | 7 | Freon/nitrogen | Instantaneous |
| Thorney Island | 8 | Freon/nitrogen | Instantaneous |
| Thorney Island | 9 | Freon/nitrogen | Instantaneous |
| Thorney Island | 12 | Freon/nitrogen | Instantaneous |
| Thorney Island | 13 | Freon/nitrogen | Instantaneous |
| Thorney Island | 17 | Freon/nitrogen | Instantaneous |
| Thorney Island | 18 | Freon/nitrogen | Instantaneous |
| Thorney Island | 19 | Freon/nitrogen | Instantaneous |
| Thorney Island | 45 | Freon/nitrogen | Continuous |
| Thorney Island | 47 | Freon/nitrogen | Continuous |
| Burro | 3 | Methane | Continuous |
| Burro | 7 | Methane | Continuous |
| Burro | 8 | Methane | Continuous |
| Burro | 9 | Methane | Continuous |
| Coyote | 3 | Methane | Continuous |
| Coyote | 5 | Methane | Continuous |
| Coyote | 6 | Methane | Continuous |

This establishes a baseline performance of our integral model for dense gas dispersion as applied to the prediction of flammable clouds, where concentrations of down to the order of 1% are of interest. Direct comparison with the performance demonstrated by Hanna et al. [1] of other similar models would be unfair and misleading however, as we have used the datasets shown in Fig. 2 for our model calibration. Nevertheless, using the statistical analysis of Hanna et al. [1], a measure of the goodness of fit is provided by

$$\mathrm{MG} = \exp\left(\frac{1}{N}\sum \log\left(\frac{C_o}{C_p}\right)\right) \tag{2.1}$$

and

$$\mathrm{VG} = \exp\left(\frac{1}{N}\sum \left(\log\left(\frac{C_o}{C_p}\right)\right)^2\right), \tag{2.2}$$

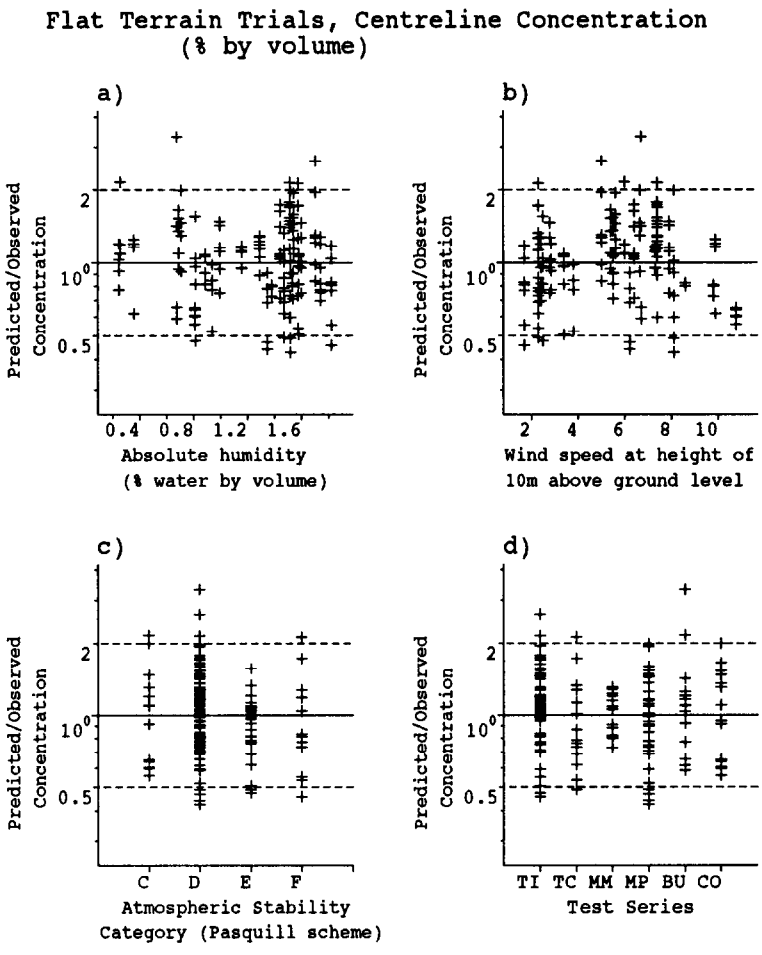


Fig. 2. A plot of model predictions relative to the observed concentrations against various parameters.

where $C_o$ is the concentration observed in the experiment, $C_p$ the concentration predicted by the model and $N$ is the number of concentration measurements.

Here, MG is a measure of the bias in the model. MG is less than 1 for a model that predicts concentrations that are too high and MG is greater than 1 for a model that predicts too low a value of the concentration. VG is a measure of goodness of fit. VG $\geqslant$ 1 for all models and the smaller the value of VG, the better is the fit of the model to the data. For a perfect model, both MG and VG would have values of 1.

The flat terrain model has MG = 0.987 and VG = 1.159. It was found that 63.6% of the predictions lie within a factor of $\sqrt{2}$ and 91.6% lie within a factor of two of the experimental data.

## 3. A model for the effects of an obstacle

The work of Britter et al. [5] demonstrated the use of a number of algorithms for the effects produced by idealised obstacles, such as infinitely long fences and isolated square or circular buildings. It is assumed that the conditions upstream of the obstacle are unaffected by its presence. The algorithms predict the conditions immediately downstream of the obstacle in terms of those immediately upstream through a series of dimensionless correlations. In this way, a single discontinuity is introduced in the calculated cloud variables to account for the complex changes that occur in reality as the cloud interacts with an obstacle. Further details of two of the more important cases are given below to illustrate the type of approach used for particular idealised obstacle arrangements.

### *3.1. Idealised solid fences*

For an infinitely long, solid fence that is perpendicular to the direction of advance of the cloud, relevant non-dimensional parameters are the ratio of the height of the cloud $h$, just upstream of the fence to the height $H$, of the fence and the Richardson number $Ri$ for the cloud upstream of the fence. The Richardson number is defined here by the relationship

$$Ri = \frac{g'h}{u^2},$$

where $g' = g(\rho_c - \rho_a)/\rho_a$, $\rho_c$ denotes the cloud density, $\rho_a$ the density of the surrounding air and $u$ denotes the cloud advection velocity.

Britter et al. [5] suggested that for clouds whose heights were less than the height of the fence,

$$\frac{w_f'}{w} = 1 + \left(\frac{H}{h}\right) Ri^{1/3} \tag{3.1}$$

and

$$h_f' = \mathrm{Max}(h, H), \tag{3.2}$$

where $w$ and $w_f'$ denote the cloud width just upstream and just downstream of the fence, and $h_f'$ denotes the cloud height just downstream of the fence. Eq. (3.1) corrects a misprint in Britter et al. [5], where the exponent in the Richardson number was inadvertently given as $-1/3$. The cloud width is increased by an amount proportional to the cube root of the local Richardson number and its height is increased to that of the fence. Clouds that are higher than the fence are assumed to be unaffected in the idealised fence algorithm.

A time delay for passage of the cloud over the fence is added. This is taken to be proportional to $H/u$, where $u$ is the advection velocity of the cloud just upstream of the fence, for both instantaneous and continuous releases. No further dilution to the cloud is considered to occur during this time period, other than that accounted for by the fence algorithm.

### 3.2. Idealised building

A similar approach is taken in accounting for the effects on a dense gas cloud when it passes an isolated circular or square building of width $W$ and height $H$. The cloud is assumed to be unaffected if its height exceeds that of the building. For lower clouds, it is assumed that both the width $w$ and height $h$ are increased to the following:

$$w'_b = \mathrm{Max}(W, w + 0.5W), \tag{3.3}$$

$$h'_b = \mathrm{Max}\left[\frac{wh + W\Delta h_0}{w'}, h\right], \tag{3.4}$$

where

$$\Delta h_0 = \mathrm{Min}\,(1, 0.1/Ri)\,H. \tag{3.5}$$

Thus, the cloud width is increased by at least half the building width and, in effect, a local increase in height produced by the frontal area of the obstacle is distributed over the dowstream width of the cloud. The term in Eq. (3.5) that is proportional to the inverse of the Richardson number is included to limit the change in height for denser clouds.

### 3.3. Composite obstacle algorithm

On a real site, the obstructions in the path of a dispersing cloud do not divide neatly into fences or isolated buildings. For example, a cloud encountering a wide single-storey building might best be treated by the 'fence' algorithm. Conversely, a much wider cloud encountering the same building might best be treated by the 'building' algorithm. Therefore, in order to produce a working dispersion model that can be used by for routine hazard assessment purposes, there is a need to produce a unified algorithm based on the dimensions of both the cloud and the obstacle. This approach has the advantage that the results of applying the model to a given site are then independent of the user. Also, the user does not have to know in advance the dimensions of the cloud in order to select the most appropriate algorithm.

The situation being considered is shown in Fig. 3, where the various symbols are also defined. Below, details are given of a single algorithm for a single, solid obstruction. For clouds that have heights that are smaller than the obstacle, the new width $w'$ and height $h'$ are defined by

$$w' = \mathrm{Min}\,(w'_f, w'_b)$$

and

$$h' = \mathrm{Max}\,(h'_0, h),$$

where

$$h'_0 = \left(\frac{w}{w'}\right)h + \left(\frac{w_1}{2w'}\right)\mathrm{d}h \quad \text{(continuous release)} \tag{3.6}$$

or

$$h'_0 = \left(\frac{w}{w'}\right)^2 h + \frac{A_1}{\pi w'^2}\,\mathrm{d}h \quad \text{(instantaneous release)}, \tag{3.7}$$

where $w_1$ is the width of the overlapping region between the cloud (after the algorithm has been applied) and the obstacle $A_1$ is the ground area that is overlapped and

$$\mathrm{d}h = F\,\mathrm{d}h_\mathrm{f} + (1 - F)\,\mathrm{d}h_\mathrm{b}, \tag{3.8}$$

with

$$\mathrm{d}h_\mathrm{f} = H - h\left(\frac{w}{w'}\right)^n, \tag{3.9}$$

$$\mathrm{d}h_\mathrm{b} = \mathrm{Min}\left(\frac{0.1H}{Ri}, H - h\left(\frac{w}{w'}\right)^n, 5h\right) \tag{3.10}$$

and

$$n = \begin{cases} 1 & \text{for a continuous release,} \\ 2 & \text{for an instantaneous release.} \end{cases}$$

Fig. 3 illustrates how $w_1$ and $A_1$ are defined for a range of possible cases. In the above, $w'_\mathrm{f}$ is the width calculated from Eq. (3.1) assuming that the obstacle behaves like a 'fence' and $w'_\mathrm{b}$ is the width calculated from Eq. (3.3), assuming the obstacle behaves like a 'building'. The weighting factor $F$ is given by

$$F = \begin{cases} 0 & \text{if } 2w'_\mathrm{b} < w'_\mathrm{f}, \\ 1 & \text{if } 2w'_\mathrm{f} < w'_\mathrm{b} \end{cases}$$

and

$$F = \frac{1}{2} + \frac{3}{2}\left(\frac{w'_\mathrm{b} - w'_\mathrm{f}}{w'_\mathrm{b} + w'_\mathrm{f}}\right) \quad \text{otherwise.} \tag{3.11}$$

Fig. 4 contains examples of the application of the algorithms for various cloud sizes relative to the building and at a range of Richardson numbers. The left-hand figure in each set shows the application of the idealised fence algorithm described in Section 3.1 in the regime in which it is valid ($w/W \ll 1$). The right-hand figures show the application of the idealised building algorithm described in Section 3.2, again in the regime for which it is valid ($w/W \gg 1$). The middle sets of figures show the results of applying our composite algorithm described above. As can be seen, this formulation has the properties that if the width obtained by treating the obstacle as a building is significantly smaller (larger) than the width that would be obtained treating it as an infinite fence, then the obstacle is treated as being fence-like (building-like). The factor $F$ allows a smooth interpolation between these limiting cases. The single algorithm has been developed so that the transition to building-like behaviour occurs at smaller

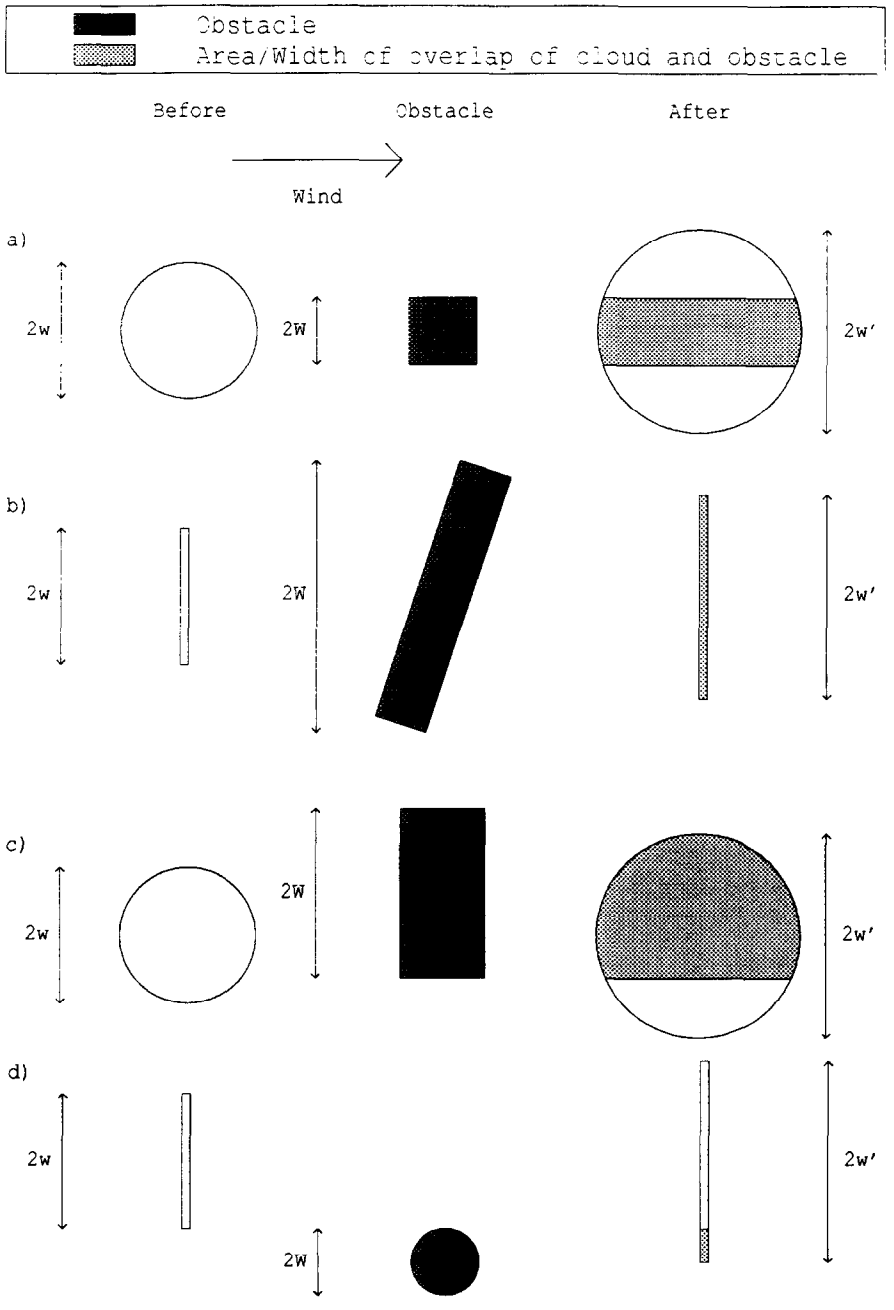


Fig. 3. Examples of instantaneous (a, c) and continuous (b, d) clouds encountering obstacles. The width/area of overlap between the obstacle and the cloud immediately downstream of the obstacle is shown, together with the half-width of the obstacle ($W$) and the half-width of the cloud immediately before ($w$) and after ($w'$) the obstacle.

widths of the cloud relative to the obstacle for larger values of the Richardson number of the cloud.

The time delay attributed to the effects of the obstacle is taken to be proportional to $(H/u)\mathrm{Min}(1, w_1/w')$ and again no additional dilution is considered to occur in this period, other than that defined by the obstacle submodel.

Porous obstacles, such as piperacks, are treated by the introduction of a solidity factor. The value of the factor is equal to the fraction of the frontal area that blocks the path of the advancing cloud.

The above formulation is applied in those cases in which the obstacle is taller than the cloud. It is assumed that there is no effect on the cloud when it is more than three times as tall as the obstacle. In the intermediate cases, $H < h < 3H$, $\mathrm{d}h$ and $w'$ are evaluated firstly assuming that the height of the cloud is equal to that of the building. Denoting these values by $h_H$ and $w'_H$, the values of $\mathrm{d}h$ and $w'$ are calculated by

$$\mathrm{d}h = G\mathrm{d}h_H$$

and

$$w'_b = G w'_H + (1 - G)w,$$

where the interpolation factor $G$ is given by

$$G = \left(\frac{3H - h}{2H}\right).$$

A reduced effect is also calculated for obstacles that do not entirely lie within the path of the cloud.

There are some problems interpreting the predictions of the model for instantaneous releases. The algorithm predicts that the cloud is unchanged until its centre passes over the centre of the obstacle, when there is an abrupt discontinuity in the cloud variables to model the complicated flow around the obstacle. For an instantaneous release, the peak concentration at any point may occur before the centre of the cloud reaches that point; usually when the leading edge of the 'box' arrives. Thus, at some locations downwind of a fence the peak concentration will appear to occur before the cloud has interacted with the obstacle. To avoid this in the model, the obstacle discontinuity is smoothed over the time between the leading edge of the cloud and the centre of the cloud passing over the obstacle.

### *3.4. Obstacle interactions*

It has been observed that there is a reduced effect produced by obstacles that have a small separation distance (less than two building heights) between them. The model accounts for this by reducing the solidity factor used in the algorithm for the downwind obstacle in direct proportion to the fraction of its frontal area that is sheltered by the first building. In this way, the predictions vary continuously as the size and position of the obstacles vary.

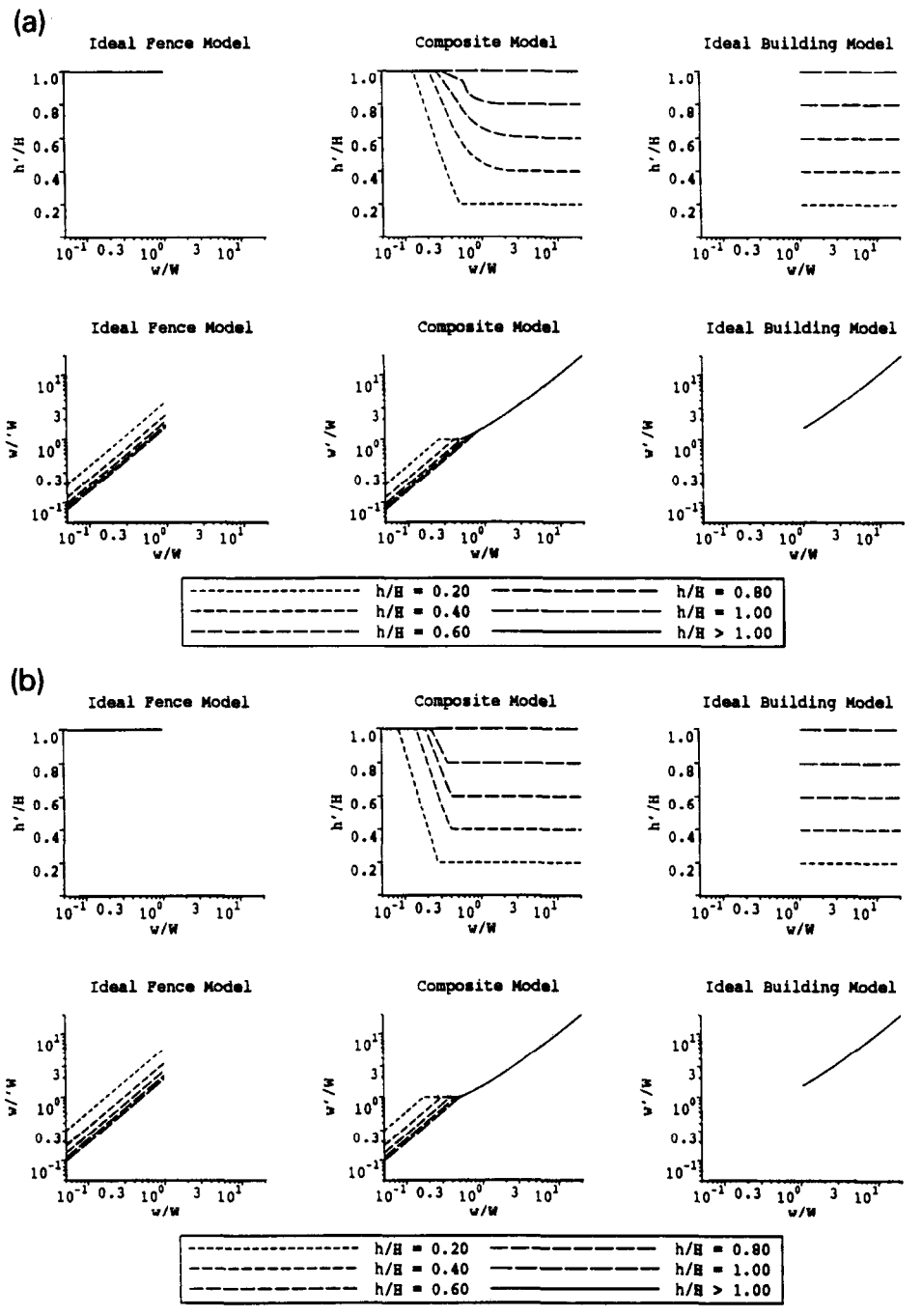


Fig. 4. The cloud heights/widths immediately after the obstacle are plotted as a function of the cloud width immediately before the obstacle, for a Richardson number of (a) 0.2, (b) 1.0, and (c) 5.0.

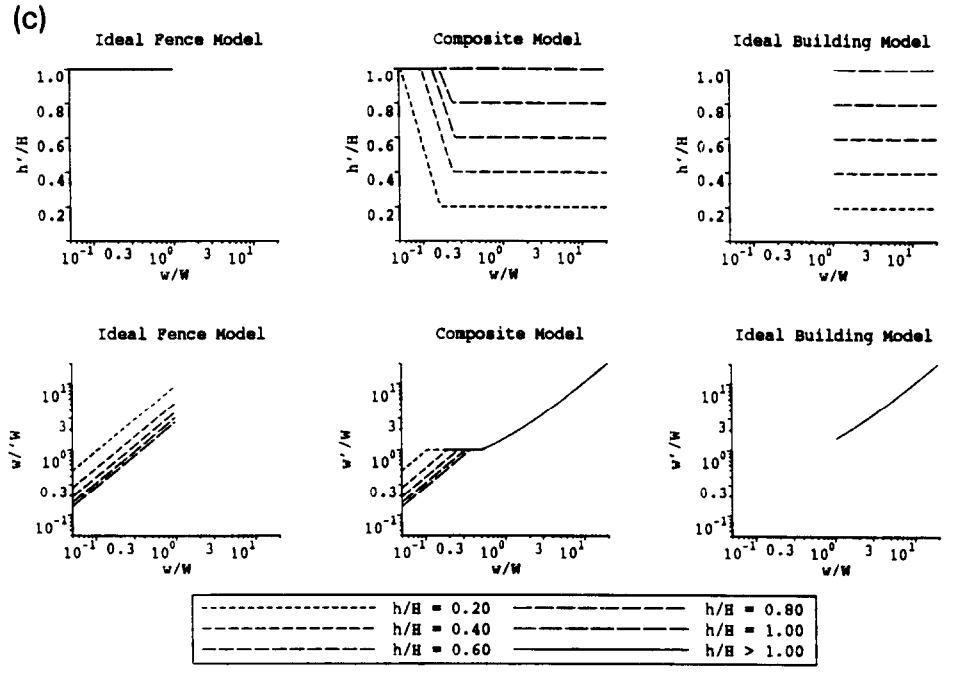


Fig. 4. (continued).

### 3.5. *Constraining obstacles*

On many installations, liquid storage tanks are surrounded by retention dykes or bunds. These are designed to prevent the spread of volatile liquid and to reduce the area of the site that is covered by the liquid in the event of a spillage. As the phase-three Thorney Island trials [14] demonstrate, they also have the property that they introduce extra dilution to certain sizes of releases as the cloud passes over the edges of the confining region. Indeed, Kothari and Meroney [15] carried out wind tunnel trials specifically to test the effectiveness of alternative designs of bund in diluting releases. Hence, a separate algorithm has been produced for bunds that surround the release location on all sides. This is referred to as the 'constraining obstacle' algorithm.

If the local height of the cloud within the bund is less than the height of the bund, then it is not allowed to become wider than the bund. On reaching the edges of the bund the edge entrainment term is also set to zero. At the downwind edge of the bund, the height increase is calculated as though the downwind edge of the bund were an ideal fence, since the cloud must lift over the bund – it cannot go around the bund as it would go around a non-constraining obstacle. The subsequent downwind evolution of the cloud is then modelled in the normal way, with the restrictions on the spread of the cloud removed.

## 4. Comparison of the model with experimental data including obstacle effects

A variety of field-scale and wind tunnel data was used to calibrate the composite obstacle algorithm. In particular, four field-scale tests from the CEC funded project 'Research on continuous and instantaneous heavy gas clouds' [2, 16] were used. (In the CEC reports describing the work carried out it is referred to as project BA.) The selected tests comprised of two jet releases and two momentum free releases encountering a short straight fence (solid or porous) approximately perpendicular to the direction of the wind. Results of ten tests from the Thorney Island field trial series [14] were also used. These were three instantaneous releases behind a solid semicircular wall, three instantaneous releases interacting with a cubic building and four continuous releases from within a rectangular fence enclosing the source. In addition, three tests from the Falcon series [17] were used. These trials consisted of continuous releases of LNG within a rectangular fence. A billboard structure was situated upwind of the source in these trials to represent the obstruction to the flow presented by a storage tank. Wind tunnel simulations from the CEC funded project BA were also used. These consisted of instantaneous isothermal dense gas clouds encountering a solid or porous fence [3]. There were 21 tests using six fence heights, two fence porosities and four Richardson numbers. Finally, 18 continuous isothermal wind tunnel tests involving either one or two bunds were used [15]. This test series included repeat tests for two different obstacle heights and three different release rates.

As for the flat terrain validation exercise, the original data reports have been used wherever possible to determine the experimental data. Results from wind tunnel experiments were only used for the calibration if the trials met criteria, such as those suggested by Meroney [18], to ensure that they are representative of full-scale behaviour. Greater emphasis was placed on the field-scale trials, but the wind tunnel data provided useful information about the effect of systematically varying the release and obstacle parameters. Unfortunately, very few of the trials used 'ideal obstacles', and there were many more examples of bund-type structures rather than isolated obstacles downwind of the source. Again, the predicted values for the ground-level centreline concentration are compared with the data available for each trial.

Fig. 5 shows the model predictions and experimental data for Thorney Island Trial 21. This involved an instantaneous isothermal release at the centre of a semicircular fence of height 5 m and radius 50 m. In this and other similar figures, the solid line denotes the predictions obtained when the obstacle submodel is included, whilst the dashed line shows the predictions without obstacle effects included in the calculation. Immediately downstream of the fence, the highest concentrations were observed above ground level and compared to an equivalent release over flat terrain concentrations are reduced by more than a factor of two. The reduction in concentration is captured by the model. Fig. 6 shows the comparison for the Falcon test 1. The source is initially diluted by the upstream billboard, then the concentration is further decreased by the surrounding fence at a distance of 25 m downwind. The concentrations predicted for the arc of measuring stations situated approximately

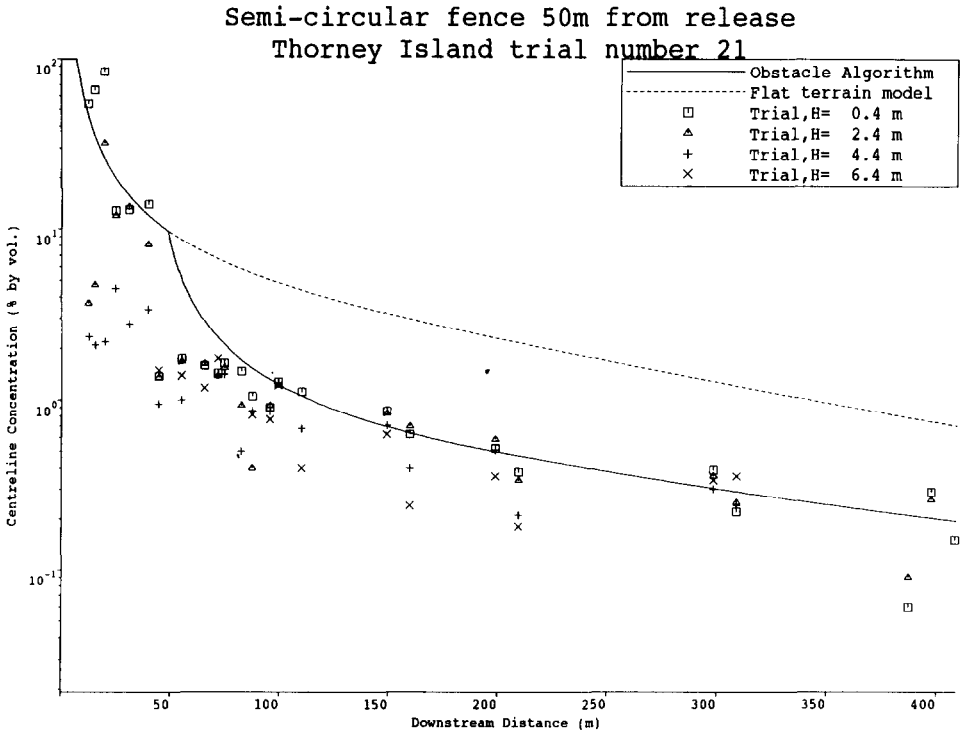


Fig. 5. An example of the obstacle algorithm applied to an instantaneous release of a freon–nitrogen mixture at ambient temperature.

150 m downstream pass through the middle of the observations. In the absence of the obstacle submodel concentrations at this location would be substantially overpredicted. The scatter in the data from the measuring stations in an arc 250 m downstream of the release is partly a reflection on the lateral concentration variation observed in the tests. It should be recalled that the predictions of the model for this case are the centreline values and so would be expected to lie above most of the data.

Fig. 7 compares the concentration predictions for CEC test 55 with the measurements. This test involved a jetted release of liquid propane from high-pressure storage. The initial stages of the dispersion of the jet were modelled using an extension of the model of Cleaver and Edwards [19] for the two-phase flow in the jet. As the cloud slows down and falls under the influence of gravity, it starts to interact with the ground. When the jet centreline is predicted to reach ground level the predicted values of the bulk radius, concentration and speed of the jet are used to create input conditions for the prediction of the subsequent dispersion using the dense gas model. Only the concentrations predicted by the dense gas model are shown in this figure. The concentrations upstream of the fence are predicted accurately by the jet model,

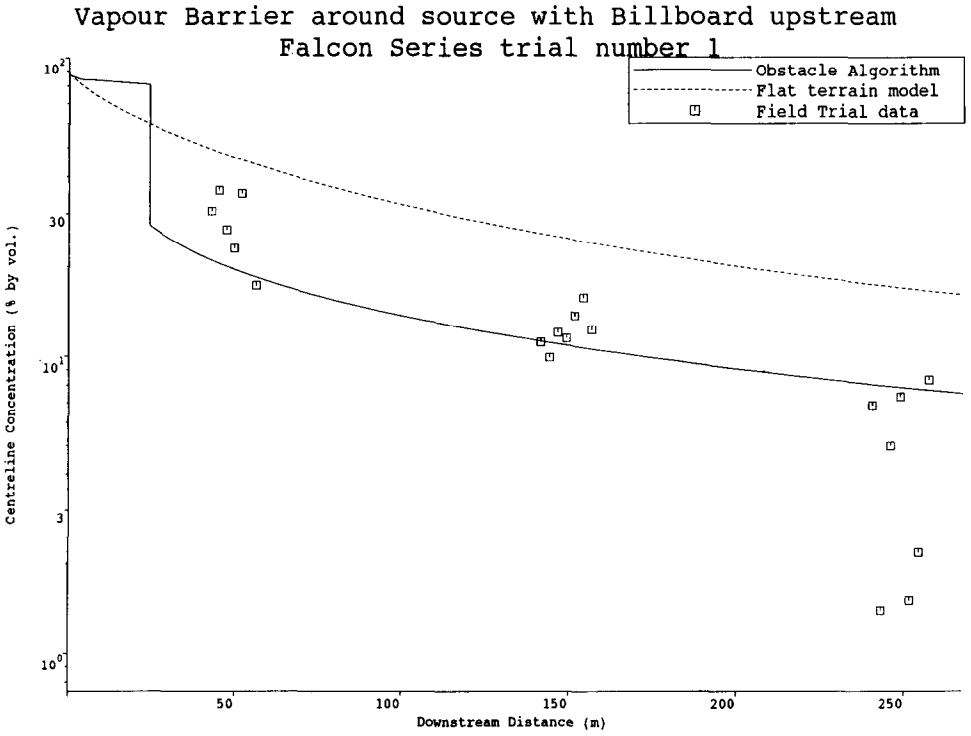


Fig. 6. An example of the obstacle algorithm applied to a continuous release of LNG vapour.

justifying the use of the jet source calculation. Immediately downstream of the fence, the predictions underestimate some of the measurements, although there is some scatter in the experimental data. However, by 15 m further beyond the fence (that is, in excess of 5 fence heights further downstream) the predictions are again in agreement with the data.

Fig. 8 shows a comparison of the observed and predicted concentrations from all the above trials. As with the flat terrain model, the solid line shows perfect agreement between model and experiment and the dashed lines represent differences of a factor of two. The level of accuracy is slightly worse than for the flat terrain model with MG = 0.910 and VG = 1.191; 61.1% of the predictions lie within a factor of $\sqrt{2}$ and 91.2% lie within a factor of two.

The model will be used for predicting dispersion of dense flammable gases on sites. Some experimental results are available for dispersion over such terrain. For example, four continuous isothermal wind tunnel tests were carried out in which the releases encountered a tank farm or a model of a refinery [20, 21]. The tank farm was modelled well by treating each tank as a separate individual obstacle. The refinery was modelled by ignoring all but the largest obstacle, which was a large structure consisting of several tanks connected by pipe work. Fig. 9 shows the experimental

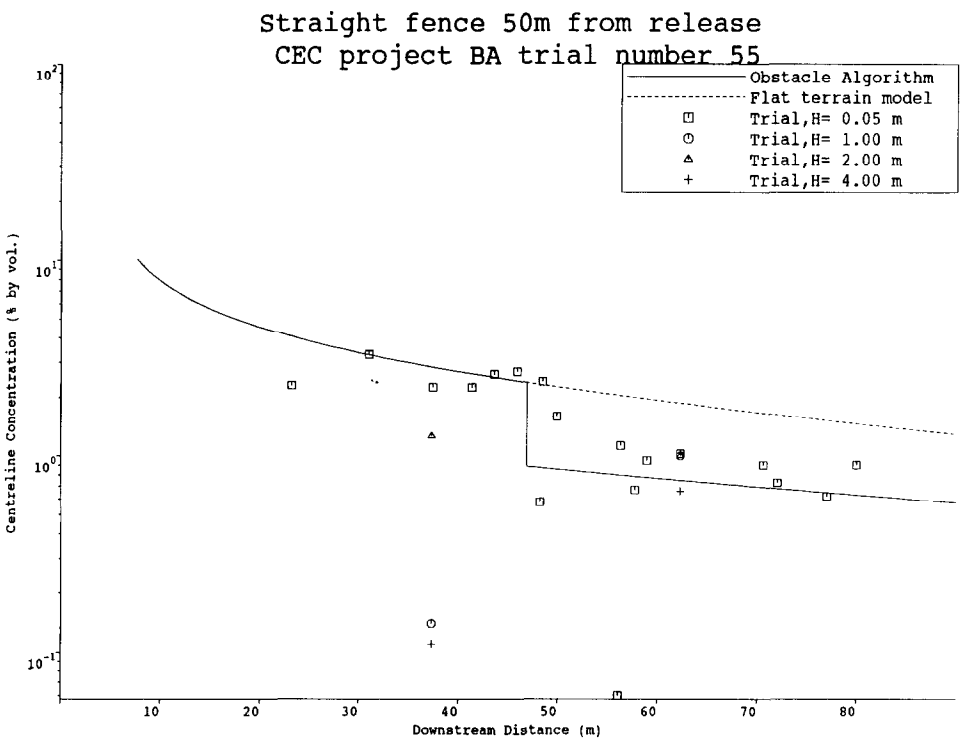


Fig. 7. An example of the obstacle algorithm applied to a continuous jetted release of cold propane.

results and model predictions with no obstructions and with only the largest building modelled. The predictions obtained using the obstacle algorithm are consistently better than the predictions obtained using the flat terrain model.

Fig. 10 gives an illustration of the ground-level concentration contours predicted by the model for two further tests from the CEC project BA. Test 55 was another jetted two-phase propane release, whereas test 58 was a propane release into a cyclone that gave a low momentum dense vapour source. The different mode of generation of the two clouds is one of the factors that lead to a difference in the predicted cloud widths. The positions of the masts are also shown in this figure, with those locations at which a concentration in excess of the selected value was detected are marked by a star and those where a smaller concentration was detected are marked with a cross. Unfortunately, there were not sufficient number of mast locations to obtain an unambiguous definition of the width of the observed concentration contour. However, if it is assumed that the cloud is symmetric about the mean wind direction, shown in the figure, then it is seen that the width predicted by the model is in good agreement. Similar results were obtained for other tests where data are available on the width of the cloud. However, this is an area where more data would be useful.

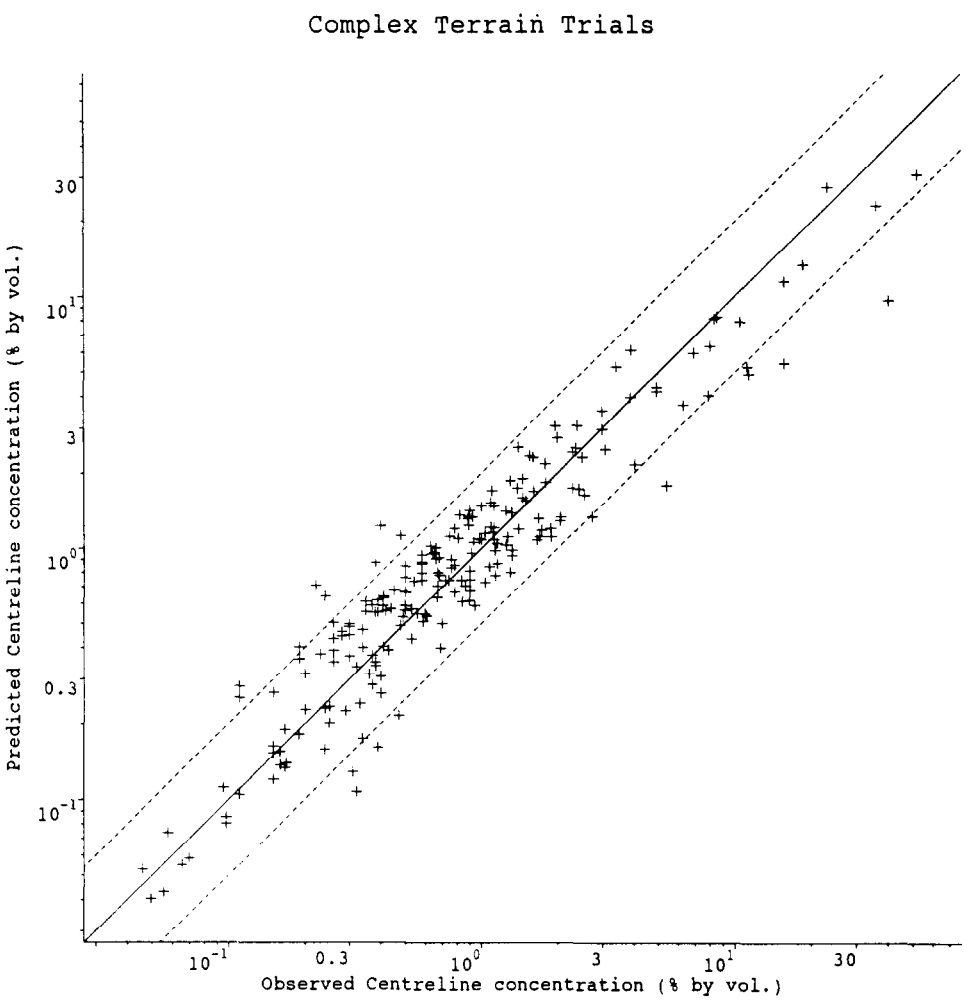


Fig. 8. A plot of the measured against the predicted concentrations for field-scale and wind tunnel trials involving obstacles.

## 5. Discussion

The comparison of the model with the flat ground data provides a reference level on the agreement that has been obtained between the predictions of the model and the data. Differences of up to a factor of two are apparent. In part, this is an inevitable reflection on the inherent uncertainty involved in making measurements on such flows. This is illustrated in the spread of measurements obtained by Hall et al. [3] during replications of the same release configuration in a wind tunnel.

A composite obstacle model has been produced. Its predictions have been compared with a range of field trial and wind tunnel data. The level of agreement is almost

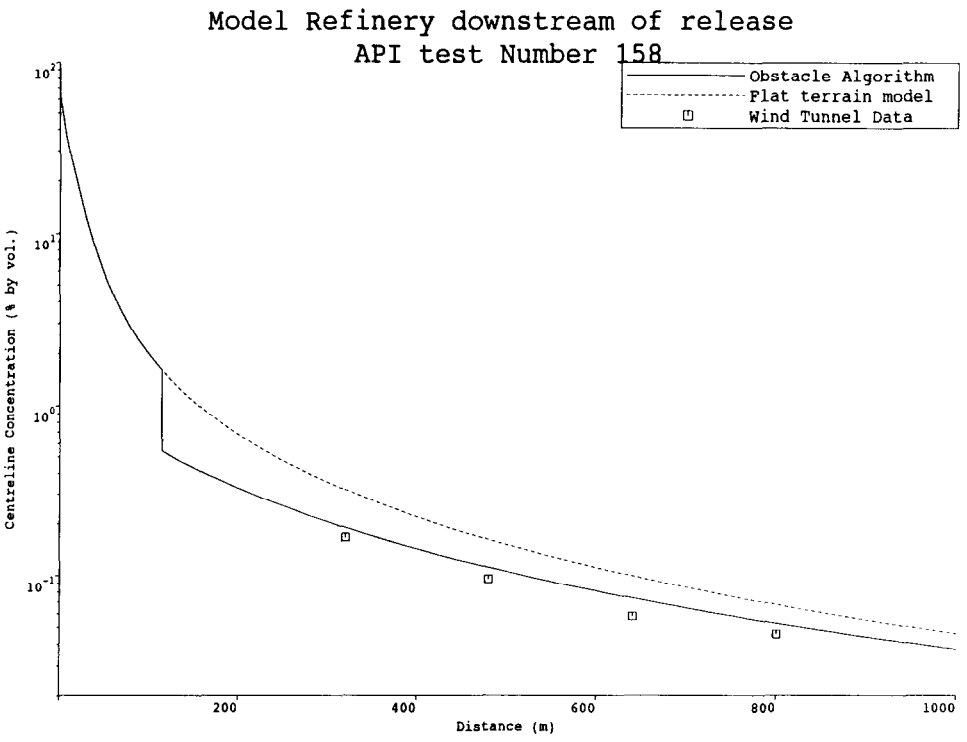


Fig. 9. An example of the model applied to a release on a complex site. The predictions of the flat terrain model and the obstacle algorithm applied to the largest structures are shown.

as good as the comparison of the flat terrain model with data. This result is encouraging. It is also the case that a better estimate of the dispersion at a site can be obtained by using our composite obstacle model than by ignoring the presence of the large obstacles. However, it should not be forgotten that this model does not attempt to solve for the flow in the neighbourhood of the obstacle. It introduces a step change in parameter values to account for the effects of the obstacle on the subsequent dispersion. In that sense, the obstacle model provides a set of equivalent 'pseudo-conditions' with which to continue the calculation (rather like the equivalent starting conditions used for an underexpanded sonic jet). Although the results to-date have not indicated any severe restrictions, it may be unwise to use the predictions of the model within a few obstacle heights downstream of an obstruction other than as indicative values. If it were ever critical to know more information in these regions, then it would require a more sophisticated modelling approach or wind tunnel tests to examine these regions of the flow.

One final point on the application of this model to real sites is that in order to complete the specification of a site, it is necessary to decide on which of the obstacles is to be modelled separately. One way of doing this is to obtain a prediction for the dispersion of a release assuming flat terrain. An area of influence can then be

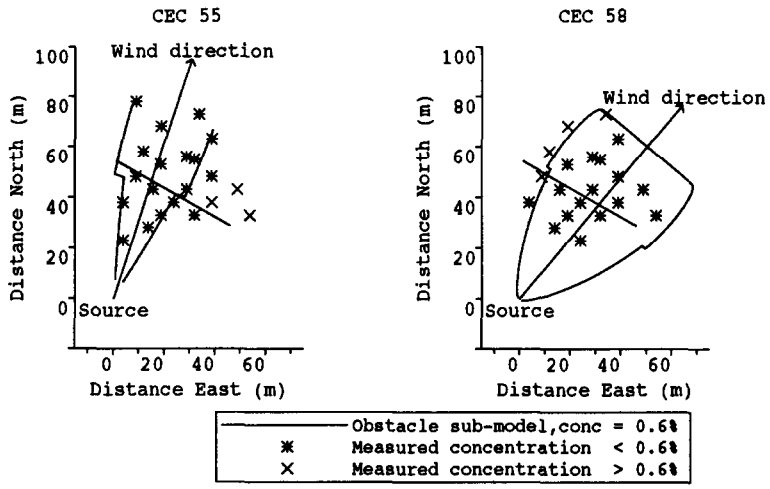


Fig. 10. A comparison of the measured and predicted cloud area for two of the CEC project BA field trials. Test 55 is a jet release, test 58 is a low momentum release.

defined and those obstacles whose heights are greater than a third, say, of the predicted height of the unobstructed cloud are treated separately. The remaining small obstructions and obstacles are represented by an increased value of the local surface roughness. A prescriptive method of defining this roughness has been developed, but further data are required to validate or refine this approach. Until such data are available some idea of the robustness of this approach can be gained by varying the factor of one- third. If small differences in this cut-off value produce large differences in dispersion predictions then the results would have to be treated with great caution.

## 6. Conclusion

It has been shown how a number of separate algorithms for the effects of obstacles on dispersion may be combined into a single algorithm that enables predictions to be made for dispersion over a typical industrial site. The complete model has been compared with results from a number of idealised field trial and wind tunnel experiments and has been shown to have a similar level of accuracy to the flat terrain model, though over a more limited range of data. This suggests that modelling the effects of obstacles by such an algorithm within a simple box model for dense gas dispersion is worth further consideration.

## Acknowledgements

The authors would like to thank Dr. R.E. Britter for providing the separate algorithms to model the effects of a fence and a building. They would like to thank

Mr. Alf Mercer of HSE and Dr. David Webber of AEA Technology for useful comments on this paper. Finally, the authors would also like to thank British Gas, plc for its permission to publish this paper.

## Appendix A: Mathematical formulation of the model

### *A.1. Governing equations*

The following set of ordinary differential equations are solved for the dispersion of a dense gas cloud over flat terrain:

$$\frac{dM}{dt} = \frac{dM_E}{dt} + \frac{dM_T}{dt}, \tag{A.1}$$

where

$$\frac{dM_E}{dt} = \rho_a \, \mathrm{Max}(U_{EP}, \gamma U_{ED}) \begin{pmatrix} 2\pi RH \\ 2UH \end{pmatrix} \begin{matrix} \text{(Inst. release)} \\ \text{(Cont. release)} \end{matrix} \tag{A.2}$$

and

$$\frac{dM_T}{dt} = \rho_a \, \mathrm{Min}(U_{TP}, U_{TD}) \begin{pmatrix} \pi R^2 \\ 2UR \end{pmatrix} \begin{matrix} \text{(Inst. release)} \\ \text{(Cont. release)} \end{matrix} \tag{A.3}$$

$$\frac{dR}{dt} = \mathrm{Max}\,(U_{EP}, U_{ED}), \tag{A.4}$$

$$M\frac{dU}{dt} = F_e \frac{dM_E}{dt}(\bar{U}(H) - U) + F_T \frac{dM_T}{dt}(U(H) - U) \tag{A.5}$$

$$M\frac{dh}{dt} = \frac{dM_E}{dt}(h_\infty - h) + E_f \begin{pmatrix} \pi R^2 \\ 2UR \end{pmatrix} \begin{matrix} \text{(Inst. release)} \\ \text{(Cont. release)} \end{matrix} \tag{A.6}$$

The symbols have the following meanings for instantaneous/continuous releases, respectively:

| | |
|---|---|
| $x$ | downstream distance |
| $y$ | crosstream distance |
| $z$ | distance above the ground level |
| $t$ | time |
| $M$ | total mass/mass flux of air entrained |
| $M_E$ | mass/mass flux of air entrained through edges of cloud |
| $M_T$ | mass/mass flux of air entrained through top of cloud |
| $\rho_a$ | density of air |
| $R$ | radius/half-width of cloud |
| $U$ | velocity of cloud |
| $H$ | height of cloud |
| $U(H)$ | wind speed at height $H$ |
| $\bar{U}(H)$ | average wind speed between ground level and height $H$ |

$U_{EP}$ edge entrainment velocity due to atmospheric (passive) dilution
$U_{ED}$ edge entrainment velocity due to gravity-driven dilution
$U_{TP}$ top entrainment velocity due to atmospheric (passive) dilution
$U_{TD}$ top entrainment velocity accounting for density suppression of mixing rates
$h$ enthalpy per unit mass of cloud
$h_\infty$ enthalpy per unit mass of ambient air

Eq. (A.1) represents the conservation of mass, whilst Eqs. (A.2) and (A.3) define the entrainment rates of air through the edge and top of the cloud, respectively. Eq. (A.4) controls the lateral spread of the cloud. Eq. (A.5) is a momentum relation to determine the cloud advection rate. Eq. (A.6) is an energy relation, including an allowance for the amount of heat $E_f$, that is transferred per unit time to the cloud per unit area of underlying surface. This is taken to be the maximum of the rate calculated assuming either forced or natural convection. The values of the model parameters $F_e$ and $F_t$ are given in Section A.3.

Also, the following subsidiary algebraic equations are used to define terms that appear on the right-hand sides of Eqs. (A.1) to (A.6):

$$U_{ED} = K\sqrt{g'H}\left(1 - \frac{1}{Ri}\right), \tag{A.7}$$

$$U_{EP} = S_y \frac{d\sigma_y}{dt} = S_y U \frac{d\sigma_y}{dx}, \tag{A.8}$$

$$U_{TD} = \frac{1}{Ri}(\alpha^2 U_*^2 + \beta^2 W_*^2)^{1/2}, \tag{A.9}$$

$$U_{TP} = S_z U \frac{d\sigma_z}{dx}, \tag{A.10}$$

$$Ri = \frac{g'H}{U_*^2}, \tag{A.11}$$

$$W_*^3 = \frac{E_f gH}{C_p \Theta \rho_a}, \tag{A.12}$$

$$\Theta = \tfrac{1}{2}(T_{ground} + T_{cloud}) \tag{A.13}$$

and

$$g' = \frac{g(\rho - \rho_a)}{\rho_a}, \tag{A.14}$$

where the following symbols have been used:
$g$ acceleration due to gravity
$C_p$ specific heat capacity of cloud at constant pressure
$\rho$ density of cloud
The values of the model parameters $\alpha$, $\beta$, $\gamma$, $S_y$, $S_z$ are given in Section A.3.

These equations are solved to determine bulk values of the cloud parameters. Profiles are then imposed over the cloud in the form of a central core region, having properties such as the concentration and temperature equal to their bulk values, together with diffuse edges in the vertical and horizontal directions. Terminating cosine profiles are used, as in Cleaver and Edwards [19]. The extent of the profile in the horizontal and vertical directions are determined from the local values of $\sigma_y$ and $\sigma_z$, respectively.

### *A.2. Source specification*

A separate algorithm is included to calculate a set of representative conditions that described the effective source for a continuous low momentum vapour release. These take the following form:

$$R_s = R_o \left\{ 1 + \mathrm{Max}\left( \frac{K\sqrt{g'_o H_o}}{U_o}, \frac{\sigma_y(R_o)}{R_o} \right) \right\} \tag{A.15}$$

$$M_{SE} = 2\gamma_s U_s H_s R_s \rho_a, \tag{A.16}$$

$$M_o + M_{SE} = 2U_s H_s R_s \rho_a, \tag{A.17}$$

and

$$U_s = \bar{U}(H_s), \tag{A.18}$$

where the subscript o refers to the vapour source and s the effective source used in the subsequent dispersion calculation. Eq. (A.15) defines the width of the equivalent source, Eq. (A.16) the mass of air entrained into the source and Eq. (A.17) expresses the mass conservation. It is assumed that the cloud leaves the source region at a speed given by the average of the wind speed over the cloud height. The value of the model parameter $\gamma_s$ is given below.

### *A.3. Values of the model parameters*

There are 9 numerical constants appearing in the model formulation, 8 for the dispersion model and 1 for the effective source. The calibration exercise produced the following set of values for these parameters: $K = 1.000$, $\alpha = 1.105$, $\beta = 4.557$, $\gamma = 0.701$, $S_y = 0.700$, $S_z = 0.7254$, $F_T = 0.55$, $F_E = 0.55$ and $\gamma_s = 0.4906$.

## References

[1] S.R. Hanna, J.C. Strimaitis and J.C. Chang, Hazard response modelling uncertainty (A quantitative method). Vol. 2, Evaluation of Commonly-used Hazardous Gas Dispersion Models, September 1991.

[2] M. Nielsen, Dense gas field experiments with obstacles, J. Loss Prev. Process Ind., 4 (1991) 29–34.

[3] D.J. Hall, V. Kukadia, S.L. Upton, Repeat variability in instantaneously released heavy gas clouds dispersing over fences – Some wind tunnel model experiments, Warren Spring Laboratory Report LR 805 (PA), 1991.

[4] M. Schatzmann, K. Marotzke and J. Donat, Research on instantaneous and continuous heavy gas clouds. EV 4T-0021-D Final Report, Univ. of Hamburg, 1990.
[5] R.E. Britter, R.P. Cleaver and M.G. Cooper, Development of a simple model for the dispersion of denser-than-air vapour clouds over real terrain, British Gas, MRS E 622, May 1991.
[6] D.M. Webber and S. Jones, Dispersion modelling. The safe handling of pressure liquified gases – Consequence analysis and prevention, IPC Conference, Inn on the Park, London, 26–27 November 1992.
[7] R.J. Harris and M.J. Wickens, Understanding vapour cloud explosions – An experimental study, Inst. Gas Engineers Publication No. 1408, 1989.
[8] R.J. Carpenter, R.P. Cleaver, P.J. Waite and M.A. English, The calibration of a simple model of dense gas dispersion using the Thorney Island Phase I trials data, J. Hazard. Mater., 16 (1987) 293–313.
[9] J.S. Puttock, The development of the HEGABOX/HEGADAS dispersion models for hazard analysis. Published by AIChE, Center for Process Studies, International Conference on Vapour Cloud Modelling, Cambridge, MA, 2–4 November 1987.
[10] J. Havens, Review of dense gas dispersion field experiments, J. Loss Prev. Process Ind., 5 (1992) 28–41.
[11] H. Witlox, Recent developments in heavy gas dispersion, Proc. Internat. Conf. on Modeling and Mitigating the Consequences of Accidental Release, AIChemE, New Orleans, 20–24 May 1991.
[12] R.E. Britter, GASTAR User's Manual, CERC Ltd, Cambridge, 1990.
[13] D.J. Wilson, Accounting for peak concentrations in atmospheric dispersion for worst case hazard assessments. Proc. Internat. Conf. on Modeling and Mitigating the Consequences of Accidental Release, AIChemE, New Orleans, 20–24 May 1991.
[14] J. McQuaid and B. Roebuck, Large scale field trials on dense vapour dispersion, Final Report on contracts 029SRUK and 036SRUK, Report No. EUR10029, Commission of the European Communities, Brussels, 1985.
[15] K.M. Kothari and R.N. Meroney, Accelerated dilution of liquefied natural gas plumes with fences and vortex generators, Final Report to GRI under contract No. 5014-352-0203, CER81-82KMK-RNM9, May 1982.
[16] M. Heinrich and R. Scherwinski, Propane releases under realistic conditions – Determination of gas concentrations considering obstacles, Tüv Report, 1991.
[17] T.C. Brown, R.T. Cederwall, S.T. Chan, D.L. Ermak, R.P. Koopman, K.C. Lamson, J.W. McLure and L.K. Morris, Falcon Series Data Report, 1987 LNG Vapour Barrier Verification Field Trials, Final Report number 1990 GRI-89/0138 prepared under contract no. 5088-252-1704 for GRI and US Dept. of Transportation, June 1990.
[18] R.M. Meroney, Guidelines for fluid modelling of liquified natural gas cloud dispersion. Vol. 2: Technical support document, Final Report (August 1984–October 1985), Report no. GRI-86/1020.2 prepared under contract no. 5083-252-0962 for GRI.
[19] R.P. Cleaver and P.D. Edwards, Comparison of an integral model for predicting the dispersion of a turbulent jet in a crossflow with experimental data, J. Loss Prev. Process Ind., 3 (1990) 91–96.
[20] R.L. Petersen and M.A. Ratcliff, Effect of Homogeneous and Heterogeneous Roughness on Heavier-than-air Gas Dispersion, Vol. 1, API publication no. 4491, March 1989.
[21] R.L. Petersen and M.A. Ratcliff, Effect of Homogeneous and Heterogeneous Roughness on Heavier-than-air Gas Dispersion, Vol. 2 – Supplemental Appendices, API publication no. 4492, March 1989.